This article has been accepted for publication in IEEE Journal of Radio Frequency Identification. This is the author's version which has not been fully edited and content may change prior to final publication. Citation information: DOI 10.1109/JRFID.2023.3327212

Digital Spectrum Twins for Enhanced Spectrum Sharing and Other Radio Applications

Serhat Tadik[1], Kaitlyn M. Graves[1], Michael A. Varner[1], Christopher R. Anderson[2], David Johnson[3], Sneha K. Kasera[3], Neal Patwari[4], Jacobus Van der Merwe[3], Gregory D. Durgin[1]
[1]Georgia Institute of Technology [2]NTIA, Boulder, CO [3] University of Utah [4] Washington University in St. Louis

***Abstract*—This paper outlines the components of a digital spectrum twin (DST) and potential *application maps* that can inform automated or enhanced spectrum management decisions. The DST is fundamentally a map and image database, with environmental, measurement, and prediction maps that allow parallel intelligence operations to generate useful information using *aggregating rules* that operate on the twin. We demonstrate several application maps generated from measured data collections and propagation modeling associated with the POWDER platform in Salt Lake City, Utah. In total, the methods of this paper provide a blueprint for generating similar DSTs in any other radio bands and regions of the world.**

I. Introduction

Researchers in radio communications envision a future where decisions related to radio operation, spectrum sharing, and network optimization are made by artificial intelligence algorithms – or at the very least informed and improved by them. A major obstacle to this vision has always been the dizzyingly-complicated, invisible world of dynamic radio usage; the most gifted engineers have found it challenging to even visualize the radioscape, let alone glean useful operating information from an up-to-date understanding of radio frequency (RF) activity. To this end, we have developed the concept of a *digital spectrum twin* to capture, extrapolate, and inform the behavior of radio usage over a geographic region and band of frequencies.

In its most general form, a DST is a cloud-based representation of RF spectrum activity in a region, based on historical data as well as measurement updates. The purposes of the DST are to enhance spectrum sharing decisions, automate network operating decisions, provide new applications for radio users, and even help to visualize the radio activity within a geographical area. The DST concept may be applied to nearly any group of radios sharing spectrum, whether it is a cellular provider managing its many customers' radio network access, or a spectrum access service (SAS) provider facilitating spectrum sharing across a shared band, a radio dynamic zone (RDZ) operator enabling spectrum sharing tests/experiments across multiple bands and types of radio users, or a regulatory agency managing licenses and usage of spectrum across a geographic region.

This paper presents methods for constructing and maintaining a DST. First, we motivate the need for a DST by discussing the confluence of state-of-the-art spectrum access schemes, propagation modeling, and radio measurement, and spectrum sensing technology. Then, we outline the basic components of a DST, which include map formation and geospatially-referenced data relevant to maintaining a DST. Finally, we review a number of aggregating rules that use the DST to provide information to spectrum sharing schemes. These final examples are based on actual measurements and modeled data from an example DST constructed for the POWDER platform [1] in Salt Lake City, Utah, over the UHF (462.7 MHz) band. Following the approach presented in this paper, domain experts should be able to duplicate similar DSTs in other bands and/or regions of the world and enable innumerable spectrum sharing and other network/spectrum management-related experiments.

A. What is the Role of a DST in a Radio Network?

Figure 1 summarizes the basic relationship between a network or community of radio users and the DST concept [2]. In the dashed line box are the typical management services offered to radio users, which may consist of individual users, other networked radios, and passive spectrum users. The addition of a DST in Figure 1 can provide real-time and historical spectrum data that improves the operation of the network/spectrum management services, which now form a suite of potential *parallel intelligence* (PI) algorithms.

In addition to the PI1 management functions, parallel intelligence algorithms may enable additional services for radio users (e.g., location-based services [3] or spectrum metering [2]). These are labeled PI3. Another set of PI functions – labeled PI2 – must be employed to maintain the DST, providing transmitter data, measured data from radio users, and, potentially, measured data from a spectrum sensing network. In all, the architecture of Figure 1 shows clearly where the management of radio spectrum can be optimized through the integration of adaptive networking and artificial intelligence (AI) principles.

B. What are the Components of a DST?

The fundamental unit of the digital spectrum twin is the georeferenced map, a pixelated map with data that can be precisely localized in space. Because these maps feature propagation picture elements, rather than simple image pixel elements, we will refer to the individual elements of data in a rasterized geo-referenced DST map as a *proxel*. In general, as depicted in Figure 2, there are three levels of geo-referenced maps in DST operation:

DST Foundation: The foundation maps are geographical information service (GIS) data that provide all of the ge-

This work is licensed under a Creative Commons Attribution 4.0 License. For more information, see https://creativecommons.org/licenses/by/4.0/

This article has been accepted for publication in IEEE Journal of Radio Frequency Identification. This is the author's version which has not been fully edited and content may change prior to final publication. Citation information: DOI 10.1109/JRFID.2023.3327212

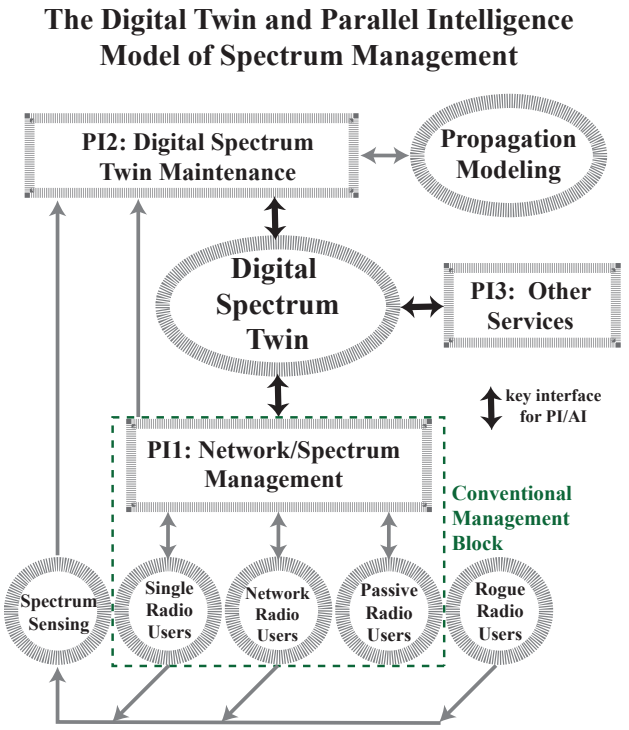

Fig. 1: Block diagram of a digital spectrum twin (DST) and its interfaces with other radios and operations in spectrum management.

ographic and environmental data that could be used in RF modeling across a broad area. These include, but are not limited to, digital elevation maps (DEMs), land-usage and/or clutter maps, road orientation maps, building footprint and/or height maps, and any other available data.

DST Core: The DST core consists of geo-referenced maps of both transmitter coverages and measured data. There are two types of transmitter maps: known transmitter (KTX) maps that are of existing transmitters and inferred transmitter (ITX) maps of emitters that are estimated based on a combination of measurements and/or inferred data (e.g., a known cellular transmitter with a measured control channel can be used to extrapolate at least intermittent received signal strength to other nearby RF bands with similar characteristics that radiate from the same transmitter.) Measurements collected and used in this level can either be associated (AM) or unassociated (UM) with a particular radio transmitter. These maps provide local ground-truth information about propagation in the region.

DST Application: The application maps produced by a DST are the aggregated results of core plus foundation maps. These maps record not only estimates of signal strength and interferers, but also estimates of variability, duty cycle, transmitter type, and even confidence in the reported values. Presumably, all of this data and more could be useful to a spectrum sharing manager or similar service provider. The information generated in the application layer can help in configuring active RFID systems for better performance by placing readers strategically and adjusting transmission power. In scenarios where multiple active RFID readers or tags are used, DST can assist in optimizing their deployment to avoid interference and maximize the efficiency of the RFID network. DST can also aid in understanding the expected signal strength in different areas of a facility, which can be useful when deploying passive RFID devices that rely on RF energy harvesting which is crucial for applications such as IoT.

The application maps may be produced as a result of instant queries (e.g., for a given region in the DST and a specified frequency band and a specific time of day, what is the expected level of interference?). Or the most current, up-to-date application maps could be maintained in memory by a DST that updates through background processes (thereby eliminating the dimension of time from storage and making "best estimates" instantly available to applications). Regardless of how an application map is stored and queried, it is constructed by aggregating behavior from all transmitter and measurement maps in the DST. The algorithm for accomplishing this depends on aggregator rules that are still open to research.

II. Background

A. Spectrum Sharing Methods

Current spectrum sharing techniques are broadly classified into the following three general categories [4]:

Opportunistic Spectrum Access (OSA): In which radios independently identify unused portions of the spectrum, access that spectrum as a secondary user, and vacate the spectrum upon the return of the primary user [5], [6]. Radios are individually responsible for spectrum sensing and avoiding interfering with the primary user. Examples include WiFi automatic channel selection [7].

Dynamic Spectrum Access (DSA): In which radios dynamically react to the current state of the spectrum environment and adapt their operating parameters in such a way as to maximize some spectrum utility metric. Radios may coordinate, collaborate, or use side-channel information (e.g., databases of known transmitter locations) to maximize the utility metric [8]. Examples include Dynamic Frequency Selection for TV White Space and WiFi [9], [10].

Administratively Managed Spectrum Access (AMSA): In which access to the spectrum as well as interference resolution is administered by a central broker or band manager. The band manager is responsible for assimilating spectrum sensor data, spectrum requests, radio operating states, interference reports, and database inputs and then determining the optimal allocation of spectrum resources to the managed radios. The leading example is the Citizens Broadband Radio Service (CBRS) in the U.S. [11], although a similar approach is used in Automated Frequency Coordination for WiFi in 6 GHz spectrum [12].

In general, the cornerstone of all spectrum sharing systems is automated measurement of the spectral environment with extremely high sensitivity and fine spatio-temporal resolution. Further, DSA and AMSA require tight control of the radio environment, while accounting for dynamic channel conditions, variable transmitter characteristics, and unknown interference

This work is licensed under a Creative Commons Attribution 4.0 License. For more information, see https://creativecommons.org/licenses/by/4.0/

This article has been accepted for publication in IEEE Journal of Radio Frequency Identification. This is the author's version which has not been fully edited and content may change prior to final publication. Citation information: DOI 10.1109/JRFID.2023.3327212

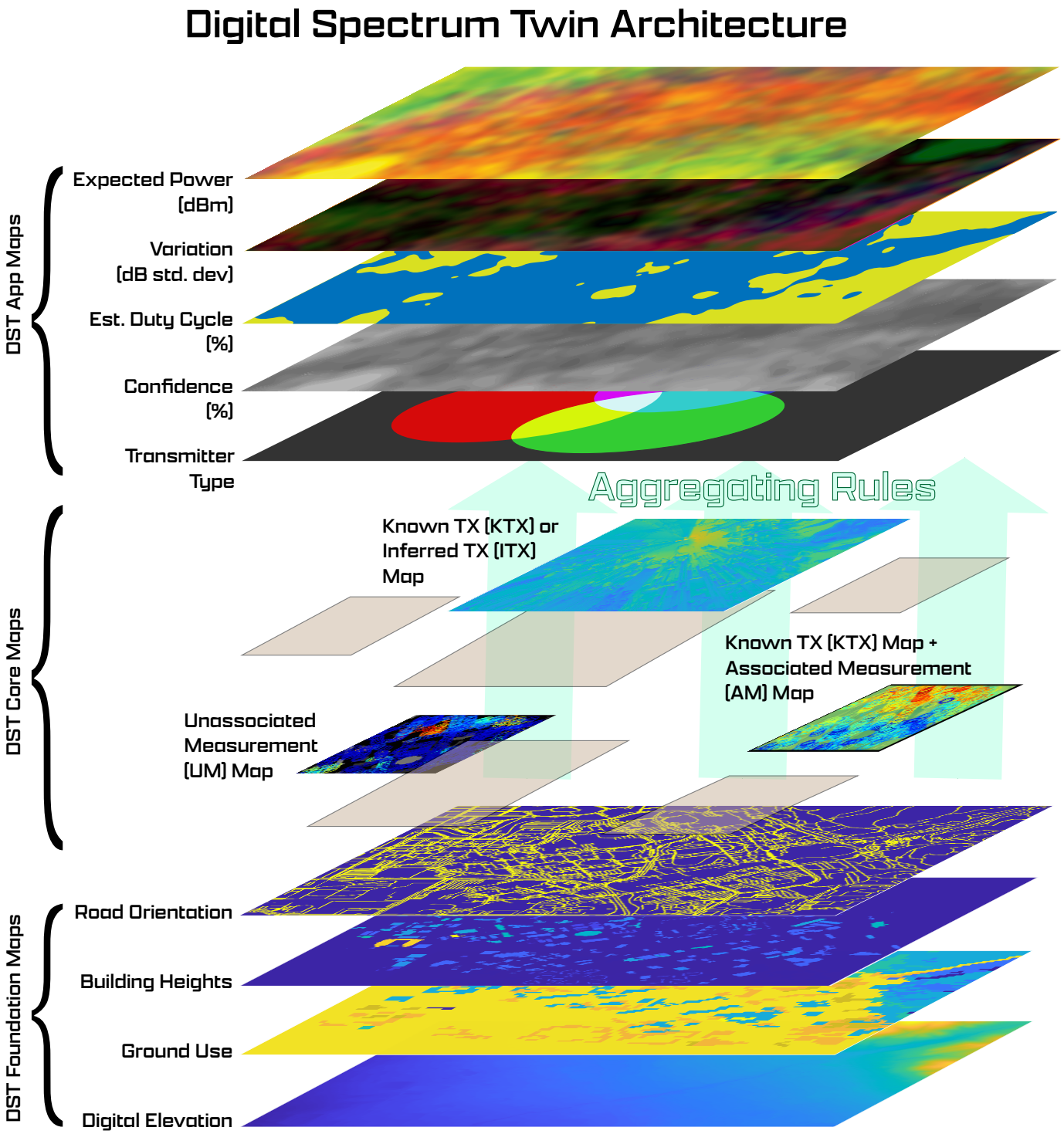

Fig. 2: A digital spectrum twin is comprised of *foundation maps* from geographical information services data as well as *core maps* that contain measurement maps (associated and unassociated with various transmitters) as well as known and inferred transmitter maps. The information of the DST is processed by *aggregating rules* to produce any number of *application maps*.

This work is licensed under a Creative Commons Attribution 4.0 License. For more information, see https://creativecommons.org/licenses/by/4.0/

This article has been accepted for publication in IEEE Journal of Radio Frequency Identification. This is the author's version which has not been fully edited and content may change prior to final publication. Citation information: DOI 10.1109/JRFID.2023.3327212

sources. Underpinning the spectrum allocation decisions are propagation and aggregate interference models. These models are often overly risk-averse in order to ensure that primary or licensed users will not experience harmful interference; however, their use results in a significant loss of overall spectrum efficiency.

B. History of Relevant Propagation Modeling

Propagation modeling is a crucial component of a DST's upkeep and maintenance as illustrated in Figure 1. The information provided by propagation modeling can help spectrum decision-makers in identifying potential sources of interference between different users by determining the range at which an emitter can transmit. Moreover, it can help identify optimal sites for new base stations to achieve maximum coverage while simultaneously ensuring minimal interference. Propagation models can be classified into three categories: empirical, theoretical, and ray-tracing models.

Empirical Models: Empirical models attempt to characterize the path loss in an environment based on factors including distance and antenna heights. This is achieved by conducting path loss measurement campaigns and determining the weights associated with each factor. The widely recognized Okumura-Hata model [13], [14] is an empirical model used to estimate median path loss, L_{med}. This model considers factors such as free space loss, L_{fs}, frequency and distance-dependent median attenuation relative to free space loss, $L_{rel}(f, d)$, loss associated with antenna heights $L(h_{tx})$, and $L(h_{rx})$, and the type of environment, L_{env} as shown in Equation (1). The Hata model builds on the Okumura model and formulates the path loss empirically.

$$L_{med} = L_{fs} + L_{rel}(f, d) + L(h_{tx}) + L(h_{rx}) + L_{env} \quad (1)$$

Empirical models can be computationally efficient, particularly if the model parameters are known. With this information, it is possible to quickly generate predictions for a georeferenced map by calculating the necessary factors and applying the model across the entire map. However, these models are applicable only within a limited range of frequencies and tend to perform optimally only when used in environments that closely resemble those in which the measurement campaign was conducted. The predictions tend to be inaccurate in dissimilar environments.

Theoretical Models: Theoretical models take into account various physical phenomena involved in signal propagation such as diffraction and ground reflection, and channel characteristics while making predictions. The Integrated Terrain (Longley-Rice) model [15] is a widely used theoretical model for predicting the propagation of radio waves over irregular terrain. It is based on a set of equations and empirical data that take into account various factors including terrain height and type, antenna heights, atmospheric conditions, frequency, and polarization. It is applicable over a wide range of frequencies up to 20 GHz. The Terrain Integrated Rough Earth Model (TIREM) [16] builds upon ITM by incorporating predictions for both land and seawater conditions, and expanding the frequency range up to 1 THz.

Ray-tracing Models: Ray tracing models involve tracing light rays as they travel from a source through a medium, such as air, and using mathematical equations to calculate the behavior of electromagnetic waves. This process yields valuable information about factors such as path loss and delay profile, making it an important propagation tool. However, due to the complexity of these calculations, ray tracing simulations can be computationally demanding and require substantial memory resources. More information about ray-tracing models can be found in [17].

Theoretical models occupy the sweet spot between empirical models and ray tracing models by offering relatively accurate predictions while keeping the complexity, memory requirements, and computation time limited. Moreover, recent work has shown that the accuracy of theoretical models can be improved when ground truth measurements are available [18], [19]. Therefore, a theoretical propagation model is the most effective way to maintain a DST over a large georeferenced map with fairly accurate predictions.

C. History of Relevant Propagation Measurement

A DST is an online representation of spectrum that is updated with a combination of measurements and models and used to provide enhanced spectrum services (sharing, localization, metering, etc.) through the use of parallel intelligence. Below we first consider relevant RF propagation measurement approaches and then discuss their tradeoff and applicability to provide input to a DST.

Dedicated Measurement Campaigns: This RF data results from designed measurement campaigns that, through careful planning, measurement, and data logging can produce insightful, reproducible spectrum measurements that help to tune models or provide measurement maps for the DST. There have been many spectral occupancy measurement campaigns performed in the past including in New Zealand, Singapore, China, and across the United States [20]–[24]. While these campaigns aimed to characterize the percentage of spectrum usage, the data gathered would be valuable for a DST.

Crowd-sourced Radio Data: This RF data is from "crowd-sourced" measurements acquired by aggregated user efforts which result in large-scale data volumes. One of the goals behind crowd-sourcing data is to increase coverage while limiting the cost [25], [26]. The radios used for crowd-sourcing RF data are typically consumer-grade devices in a live network, so there can be no guarantees about condition, RF electronic parameters, or sample selection biases which can all skew results. In fact, these devices typically have higher nonlinearities and variabilities [27], and lower sensitivity and smaller bandwidths compared to equipment used in dedicated measurement campaigns which makes it difficult to sense signals with low SNR as well as perform wideband sensing; however, the large radio densities that come with crowd-sourcing measurements can counteract those effects [28], [29]. Methods of compensating users for their time, energy, and

This work is licensed under a Creative Commons Attribution 4.0 License. For more information, see https://creativecommons.org/licenses/by/4.0/

This article has been accepted for publication in IEEE Journal of Radio Frequency Identification. This is the author's version which has not been fully edited and content may change prior to final publication. Citation information: DOI 10.1109/JRFID.2023.3327212

the quality of information collected have been proposed to incentivize users to keep participating in quality data collection [30]–[33].

Spectrum Monitoring Infrastructure: RF data from dedicated spectrum monitoring infrastructure occupies a middle ground between the scarce, valuable scientific measurement of a dedicated campaign and the low-grade, high-volume data that might be available through crowd-sourcing measurement data. Dedicated, stationary spectrum monitors continuously scan the spectrum; however, these large-scale monitoring stations are often limited in their coverage due to the costs of each station [26]. To increase coverage of the monitoring infrastructure while minimizing cost, sensor networks utilizing RFID technology or low-power sensor motes, can be employed [34]–[36].

Tradeoffs and Applicability to DST: There are many practical implementations and trade-offs that need to be taken into consideration when obtaining RF measurements. For example, specifications such as resolution bandwidth must be chosen carefully when setting up the measurement equipment. A small resolution bandwidth results in finer, more precise spectrum measurements as well as a lower noise floor; however, it also results in an increased scanning time [37]. A long scanning period is not ideal as changes in the RF environment could be missed if they occur mid-scan [28]. However, if the resolution bandwidth is too large, signals can be missed in the noise floor; therefore, there is a trade-off between the two.

Data for a DST must be collected over large bandwidths. Wideband receivers can be used; however, they are often expensive and, therefore, not practical when trying to have large areas of coverage. They also require a longer scanning period to cover the desired band. On the other hand, inexpensive consumer-grade radios or sensor motes often have limited bandwidth. However, by dividing the sensing nodes into multiple sub-bands, the cost and scanning period can be minimized while still obtaining measurements for the required frequency ranges [28], [34].

The channel uncertainties that exist due to the complexity of the RF environment have a profound impact on the quality of spectrum sensing. Spectrum monitors individually are susceptible to shadowing, multipath effects, and noise uncertainty [38], [39]. In order to reduce the impacts of fading and noise uncertainty, it is possible to average out the noise from the measurements over longer observation periods, and therefore, improve the SNR [40]. Using monitors with increased sensitivity can also combat the channel uncertainty effects, however, that may not be possible due to hardware limitations [41]. Diversity could be introduced to the system, such as through the use of MIMO antennas, to mitigate the shadowing and fading effects since each antenna would experience independent fading conditions [42]–[44]. Another way to introduce diversity gain to a spectrum monitoring system is through cooperative sensing, having multiple sensors set to collect the same data in the same region spaced at least a few wavelengths apart [38], [39], [45]. Through cooperative sensing, the overall detection sensitivity is improved with the same individual device sensitivity as the density of sensors increases [29], [45].

D. History of Relevant Spectrum Sensing and Detection Techniques

An integral part of a DST is spectrum sensing and detection, which is essential for detecting transmissions from known or unknown devices in a specific region. There are various techniques that can be used to detect the presence of such transmissions such as energy detection, radio identification-based sensing, waveform-based sensing, cyclostationarity-based sensing, and other methods [46]–[50].

Energy Detector: The energy detector method is frequently used due to its ease of use and energy efficiency. It is more flexible than other methods because it does not need any knowledge of the transmitted signal beforehand. The energy detector attempts to identify the signal by comparing the received signal strength to a threshold based on the noise floor, but it faces some challenges in identifying the threshold due to noise uncertainty, differentiating amongst transmitters, and performing in low signal-to-noise ratio environments [51]–[53].

Radio Identification-based Sensing: This type of sensing aims to identify the technology used by the transmitting device based on the signal characteristics. These characteristics could be the distribution of signal energy over the frequency spectrum and the channel bandwidth. A learned classification model trained with these features can then be employed to identify the technology used by the transmitting device. This information combined with the information obtained from other detection techniques can help identify the transmission parameters of the device [46].

Waveform-based (Coherent) Sensing: Coherent sensing leverages the known patterns or sequences available in a communication signal such as preambles, pilot sequences, and spread sequences to detect a transmission. The received signal is correlated with a known set of such sequences and results are compared to a predetermined threshold to make the final decision. This technique can only be used for detecting those transmissions containing the sequence available in the known sequence set [46], [54], [55].

Cyclostationarity (Spectral Correlation)-based Sensing: This is a technique making use of the periodicity of the signal or the moments of the signal for detection [56]–[58]. The cyclic power spectral density and spectral coherence function of the received signal contain information about the type of modulation, carrier frequencies, and pulse, and chipping rates of signals. Since different transmissions contain different information, this technique can distinguish between different transmissions [59]. Moreover, since stationary noise does not exhibit any spectral correlation or periodicity, this technique can differentiate between noise and transmissions [60].

The choice of detection technique depends on the source of measurements. Dedicated measurement campaigns with enough stationary as well as mobile measurements would enable using power-hungry, online, and coherent detection

This work is licensed under a Creative Commons Attribution 4.0 License. For more information, see https://creativecommons.org/licenses/by/4.0/

This article has been accepted for publication in IEEE Journal of Radio Frequency Identification. This is the author's version which has not been fully edited and content may change prior to final publication. Citation information: DOI 10.1109/JRFID.2023.3327212

techniques such as coherent and spectral correlation-based detection along with the energy detector. Crowd-sourced radio data would only enable using an energy detector type of detection technique as the energy consumption, and signal processing capability of user-provided radios are limited. As for the spectrum monitoring infrastructure, the choice of detection technique depends on the type of device or sensor used in the network. A low-power sensor network consisting of semi-passive RFID tags, for instance, can be used to relay digitized measurement data over a distance as long as 1 km to a central reader where any type of complex processing and detection technique can be implemented [34]. Incorporating arrays into the reader has the potential to amplify both the range and read rate of the spectrum sensors, providing further enhancements [61], [62]. The use of active sensor motes can boost the scale of sensor networks considerably enabling sensing and data collection in larger geographic regions [63].

III. DST Components

A. Georeferenced Maps and Images

The primary component of the DST is a collection of georeferenced, rectilinear maps, depicting various physical and electromagnetic attributes of the region of interest. The foundation map collection is the backbone of DST, informing all RF prediction calculations, rendering them region specific and more accurate.

The DST foundation maps for a given area comprise three types of independent maps: physical/stationary (e.g., elevation profile, building footprints and heights, ground use classification, road maps), temporal (e.g., pedestrian and automotive traffic patterns, seasonal foliage behavior, weather), and electromagnetic (e.g., channel classification, antenna patterns and look angles, blockage, and scattering parameters). Map and image generation is usually the most time-intensive element in the creation of a new DST, as defining, aligning, and combining independent maps can be a painstaking process. However, once an initial map collection is defined, it is relatively easy to add additional or make minor adjustments to existing layers beyond what was required for the minimum viable model.

Note that, when creating a collection of DST foundation maps from an aggregate of independent sources, not all sets will share accuracy and precision characteristics. If ignored, this can result in erroneous representations of the area of interest. For example, a terrain data set with a relative variance deemed acceptable by its publishers, whose errors from ground truth are relatively small when compared with the average size of measured features, could present per-pixel errors whose magnitudes rival the size of an average building height. The resulting superposition of these individual sources will not represent any realistic environment, but instead a jagged meta-terrain where buildings are deformed or engulfed by a set of impossibly tumultuous ground features.

It is therefore imperative that each individual source be characterized fully before its adoption to the map collection and implementation in the DST. It is possible, and permissible, to have maps in the DST foundation layer which are incompatible with each other, so long as they are employed independently. Consulting the providers of a map is advised when accuracy statistics are not readily available or deducible.

The most basic propagation models will only require a hybrid map of some stationary descriptors to produce an initial estimate, namely the absolute digital terrain profile (a combination of the elevation and infrastructure maps). A large variety of physical/stationary maps are available through public institutions to be used in basic research or for the public good and can be found as Geographical Information System (GIS) repositories. Using GIS manipulation software, multiple layers of ground elevation and infrastructure layouts and heights can be aligned and superimposed into a single rectilinear grid where each pixel value represents the absolute elevation of the real-world environment, like that depicted in Figure 2. By creating a collection of foundation maps by manipulating data from sources including public GIS repositories, OpenStreetMap, and the National Land Cover Database, it is possible to create a fine-tuned static depiction of the region to be simulated.

Note that distortions are inevitable when representing the curved surface of the earth as a 2D image. Therefore, it is important to choose GIS data sets that minimize earth curvature effects. The DST foundation maps for this work are generated using high-resolution LIDAR data. Taken from an airplane, the measurement reference point effectively follows along the earth's curvature, minimizing angular aberration and more readily allowing data to be fit and stitched to rectangular grids. Using public satellite imagery for microcellular region depiction is undesirable due to maximized aberrations and large resolution granularity.

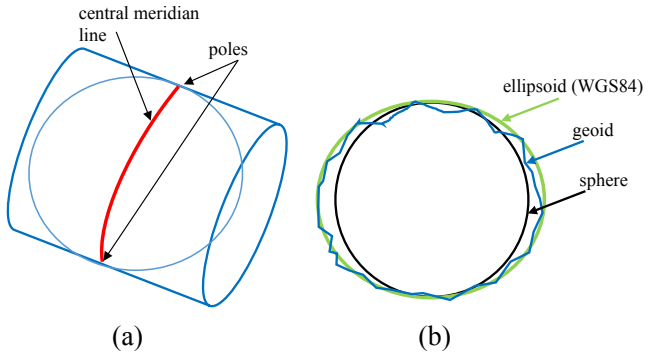

Fig. 3: (a) Transverse cylindrical projection used in UTM, and (b) the approximation of Earth's shape as an ellipsoid by WGS84.

Additionally, using Universal Transverse Mercator (UTM) coordinates for georeferencing the maps in DST is preferred because the coordinate values are localized to a specific zone and referenced by the meter, making it easily adapted to a rectilinear representation of the region. Moreover, UTM utilizes a transverse Mercator projection as depicted in Figure 3.a, which is a cylindrical projection that is transposed to align with the zone's central meridian. This projection minimizes

This work is licensed under a Creative Commons Attribution 4.0 License. For more information, see https://creativecommons.org/licenses/by/4.0/

This article has been accepted for publication in IEEE Journal of Radio Frequency Identification. This is the author's version which has not been fully edited and content may change prior to final publication. Citation information: DOI 10.1109/JRFID.2023.3327212

distortion within each UTM zone, providing a more uniform representation of the Earth's surface within the zone. This, in turn, makes it suitable for mapping purposes as distortions in shape, and distance are minimized. The traditional World Geodetic System 84 (WGS84) standard that is used by the Global Positioning System (GPS) and GIS, on the other hand, provides a global approximation to Earth's shape as illustrated in Figure 3.b. This standard can also be used to generate georeferenced maps, but further attention must be paid to coordinate precision, as truncation of finely defined angular measurements can result in serious location misrepresentation in a microcellular region. If source data is presented in WGS84, a coordinate system transfer can be easily applied within any GIS manipulation software to recast the data in a UTM system, rendering it able to be suitably described as a matrix. The WGS84 coordinate units latitude, ϕ, (in radians), and longitude, λ, (east of Greenwich, in radians) can be converted into UTM eastings, E, and northings, N, through Equations (2)–(3) [64]:

$$E = k_0 v \Bigg[A + (1 - T + C)\frac{A^3}{6} + (5 - 18T + T^2 + 72C - 58e'^2)\frac{A^5}{120} \Bigg] + 500000 \tag{2}$$

$$N = k_0 \Bigg\{ M + v\tan(\phi)\Big[\frac{A^2}{2} + (5 - T + 9C + 4C^2)\frac{A^4}{24} + (61 - 58T + T^2 + 600C + 330e'^2)\frac{A^6}{720} \Big] \Bigg\}, \tag{3}$$

where the location is assumed to be in the northern hemisphere. A location in the southern hemisphere will have the northing, $N_{south} = N + 10^7$. The scale on the central meridian is denoted k_0 and has a value of 0.9996.

$$v = \frac{a}{\sqrt{(1 - e^2 \sin^2(\phi)}}, \tag{4}$$

where $a = 6378137$ is the equatorial radius in meters, and $e \approx 0.08181919$ is the eccentricity of the ellipsoid used by WGS84.

$$A = \cos(\phi)(\lambda - \lambda_0), \tag{5}$$

where λ_0 is the longitude east of Greenwich of the origin of the rectangular coordinates and is determined as a function of the zone number, n, as illustrated in Equation (6):

$$\lambda_0 = [6(n-1) - 180 + 3]\frac{\pi}{180} \tag{6}$$

M is the true distance along the central meridian from the Equator to ϕ and is calculated as shown in Equation (7).

$$M = a\Bigg[(1 - \frac{e^2}{4} - \frac{3e^4}{64} - \frac{5e^6}{256})\phi - (\frac{3e^2}{8} + \frac{3e^4}{32} + \frac{45e^6}{1024})sin(2\phi) + (\frac{15e^4}{256} + \frac{45e^6}{1024})sin(4\phi) - (\frac{35e^6}{3072})sin(6\phi) \Bigg] \tag{7}$$

Other auxiliary variables are calculated as:

$$\begin{aligned} e'^2 &= \frac{e^2}{(1 - e^2)} \\ T &= \tan^2(\phi) \\ C &= e'^2 \cos^2(\phi) \end{aligned} \tag{8}$$

Once the conversion from WGS84 to UTM is completed, the extent of the map i.e. minimum and maximum UTM coordinates along with the cell size need to be determined. These parameters can be used to construct the header of an Esri ASCII grid file that includes the number of columns and rows, corner (or center) Eastings and Northings of the grid, the cell size, and a value to represent missing cells. The grid is then populated with actual data values such as elevations or path losses. The value associated with a given WGS84 coordinate expressed with a longitude and latitude pair can be obtained by converting the coordinate to UTM and locating it on the grid with respect to the local origin which is often the corner of the image.

IV. Construction of DST Maps

A. Classification of Measurement Maps

Regardless of how measurements are gathered, all measurement data should be organized into a georeferenced map that precisely marks location and signal strength. The map may also includes metadata about the receiver that was used to perform the measurements, the window of time over which this data was collected, and any other useful contextual information. There are two types of measurement maps:

Unassociated Measurement (UM) Maps: These maps record signal strength within a specified RF band over a known time window, but may not be associated to any particular transmitter. An example receiver providing this data might be a spectrum analyzer in the back of a moving test vehicle measuring signal power in various bands without decoding the RF signals – thus, the measured signal strength could be an estimate of signals from multiple RF transmitters and noise. Another example receiver might be crowd-sourced received signal strength indicator (RSSI) data from mobile handsets that are not fully decoding and associating individual scanning measurements.

Associated Measurement (AM) Maps: These maps record signal strength that can be directly associated with a particular radio transmitter, usually by decoding the received signal strength and verifying the identity of the transmitter. An example of this type of data might be a user device

This work is licensed under a Creative Commons Attribution 4.0 License. For more information, see https://creativecommons.org/licenses/by/4.0/

This article has been accepted for publication in IEEE Journal of Radio Frequency Identification. This is the author's version which has not been fully edited and content may change prior to final publication. Citation information: DOI 10.1109/JRFID.2023.3327212

that provides RSSI data for particular WiFi transmitters with known SSID. Another example would be the decoded control channels scanned by a cellular drive test.

At this point, it is important to note that measurements serve multiple purposes for the maintenance of a DST. The RF measurements may be used to adjust RF propagation models – an operation called *tuning*. System-wide measurements (SWM) used to tune a general RF propagation model may be referred to as macro-tuning, while localized measurements used to tune a specific transmitter's or region's propagation model may be referred to as micro-tuning.

In addition to tuning, RF measurements can also serve as an approximation of "ground truth" in a DST – superseding modeled estimates of signal strength and behavior in a measured location. For example, in a DST map of signal strengths for a certain band and region consisting mostly of a stationary transmitter's modeled data, the RF measurements associated with that transmitter can be inserted directly into the map. Small areas within the map that surround this inserted measured data can then be populated with an interpolation of measured and modeled signal strength and statistics.

Likewise, there are two types of transmitter maps in the DST core. First are known transmitter (KTX) maps. These are maps of known emitters with known parameters and, at very least, contain a complete rendering of estimated signal strength proxels across a wide area through modeling. If an AM map is associated with one of these known transmitters, then the two maps may be effectively "fused" in the DST, and a more complete blended coverage map results.

Alternately, it is possible to generate an instance of an inferred transmitter (ITX) map if the presence and transmit parameters may be inferred from spectrum measurements and estimates. Presumably, an ITX map will be able to extrapolate more accurate behavior into unmeasured proxels of the DST than simply blending unassociated measurement (UM) maps into an application map.

V. Example Aggregating Rules

The physical, temporal, and electromagnetic information in the DST foundation layer and transmitter and measurement maps in the DST core layer are aggregated with certain rules to generate useful information such as expected received signal strength, variation, duty cycle, transmitter type, and confidence in the DST application layer.

Some existing approaches to generate expected received signal strength (or coverage) map include measurement-based methods that leverage spatial interpolation techniques such as linear interpolation [65], and Kriging method [66]–[68], or a Gaussian process for regression (GPR) technique [69] implemented on collected RSS data. However, these mainly empirical approaches do not consider the propagation and channel characteristics explicitly. Their performance is largely dependent on the number and distribution of the collected data points. Therefore, they are convenient primarily when crowdsourced data is available. An approach that leverages both theoretical propagation models and measurements is proposed for aggregation in this section.

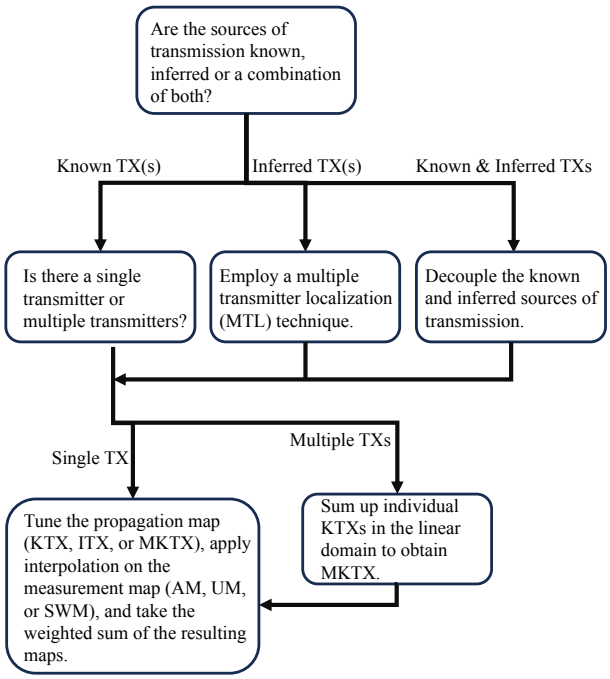

Fig. 4: A flowchart summarizing the process of aggregating expected received signal strength.

A. Aggregation of Expected Received Signal Strength

Aggregating rules may vary between different scenarios including single and multiple known TXs, inferred TXs, or a combination of KTXs and ITXs:

Single KTX: When only one transmitter is known to be operating across the region of interest and its location and parameters are known, the expected received signal strength can be estimated using the preferred propagation model, constituting the KTX map. In the presence of measurements associated with the transmitter, i.e., when an AM map is available, these predictions can be micro-tuned with an approach similar to the augmented modeling approach proposed in [18]. Moreover, these measurements serve as an accurate reference, allowing for the interpolation of signal strength in nearby unmeasured areas, thus providing estimates for the proxels in the vicinity. In general, the expected received signal strength can be computed using a weighted combination of the interpolated measurement values and the micro-tuned signal strength predicted by the propagation model as outlined in Equation (9):

$$\begin{aligned} KTX' &= tune(KTX, AM) \\ AM' &= interpolate(AM, d_{max}) \\ E[RSS] &= weight(KTX', AM', d_p, d_{max}), \end{aligned} \tag{9}$$

where d_{max} is the maximum allowable distance from a measured proxel that is to be interpolated, and $E[RSS]$ is the expected received signal strength. The $weight(\cdot)$ function

This work is licensed under a Creative Commons Attribution 4.0 License. For more information, see https://creativecommons.org/licenses/by/4.0/

This article has been accepted for publication in IEEE Journal of Radio Frequency Identification. This is the author's version which has not been fully edited and content may change prior to final publication. Citation information: DOI 10.1109/JRFID.2023.3327212

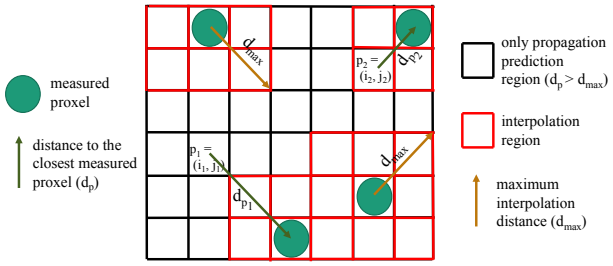

Fig. 5: A simple illustration of maximum interpolation distance, d_{max}, and distance to the closest measured proxel, d_p.

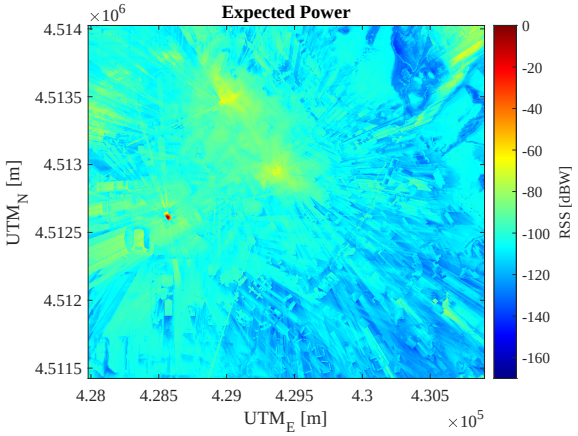

Fig. 6: Aggregated expected power map obtained from three KTXs tuned and weighted with the corresponding AM maps. The frequency of operation is 462.7 MHz in the UHF band.

provides a weighted sum of the KTX' and AM' maps and depends on the distance, d_p, between a given proxel $p = (i, j)$ and the closest measured proxel such that the interpolated measurements are weighted less as the distance to the closest measured proxel increases. If d_p is larger than the d_{max} used in the interpolation step for a given proxel, the corresponding $E[RSS]$ is equal to KTX'_p.

Multiple KTXs (MKTX): When multiple KTXs with known parameters are present, their individual KTX maps can be combined to create a general propagation map, namely MKTX. The aggregation of the individual KTXs can be as straightforward as adding the estimated received powers of various transmitters in the linear domain as shown in Equation (10),

$$MKTX = \sum_{i=1}^{m} KTX_{i,linear} \tag{10}$$

where m is the number of KTXs known to be transmitting in the region.

The system-wide measurements (SWM), if available, can be used to macro-tune the general map to enhance the accuracy of predictions. The aggregation of $E[RSS]$ then follows the process outlined in Equation (9), except that MKTX is used instead of KTX and SWM is used instead of AM. Alternatively, individually tuned KTX maps can be combined to attain a tuned general map as depicted in Figure 6.

Inferred TXs (Rogue Device Detection Mode): If an unexpected transmission is detected using the energy detector technique from an UM map while no known transmitter is operating (i.e., in the rogue device detection mode [2]), existing multiple transmitter localization (MTL [70], [71]) techniques can be employed to localize the transmitters and infer the transmission parameters, for example, gain pattern, orientation, and transmit power [72]. One reasonable and time-efficient localization approach is to find the local maxima of the signal strength measurements compared to a predefined threshold and treat the problem as a K transmitter localization problem using the signal strength measurements at the vicinity of the local maxima [73]. Another approach is to convert an image of sensor readings (the UM map) to an image of peaks where each peak implies a transmitter. A peak-finding / object detection method is used consequently to infer unknown transmitter location and signal strengths [74]. The advantage of these approaches is that they can be used for an unknown number of transmitters, either single or multiple.

If the detection is performed with coherent, radio-identification, or spectral correlation-based techniques, additional information obtained from these techniques can be used along with signal strength information to infer location and transmission parameters about the potential source of transmission more confidently.

Once one or more unknown sources of transmission are detected, ITX maps can be generated for each source. Next, ITX and UM maps can be utilized in the same way as KTX and AM maps as outlined in Equations (9)–(10) to obtain expected received signal strength predictions throughout the map.

Combinations of KTXs & ITXs: When a set of KTXs are operating in the region along with a set of unexpected sources of transmission, one approach could be to first decouple the known and unexpected (unknown) signal strengths at a given proxel with the help of the UM, and general KTX map (either KTX or MKTX) using Equation (11):

$$\widetilde{UM}_{lin} = max(0, UM_{lin} - MKTX_{lin}), \tag{11}$$

where $\widetilde{UM}_{lin}$ is the decoupled signal strength map associated with unexpected sources only. Once this map is obtained, a similar process for single or multiple transmitter localization can be implemented. If unexpected transmissions are detected with a non-energy detector technique, additional information can be used for an easier and more accurate inference. Once all the transmitters are known to the DST, the same procedure of constructing a macro-map and tuning it can be applied with the larger set of transmitters.

B. Aggregation for Signal Variation

The variation in RF signal strength can be attributed to a range of factors, including ambient noise, noise due to the receiving device, interference, changes in transmit power, small-scale fading, and shadow fading. A signal variation map

This work is licensed under a Creative Commons Attribution 4.0 License. For more information, see https://creativecommons.org/licenses/by/4.0/

This article has been accepted for publication in IEEE Journal of Radio Frequency Identification. This is the author's version which has not been fully edited and content may change prior to final publication. Citation information: DOI 10.1109/JRFID.2023.3327212

in the application layer along with the expected power map provides information regarding one standard deviation confidence interval, $(\mu - \sigma)$ to $(\mu + \sigma)$, for possible signal strength values at a certain location where μ is the expected RSSI, and σ is the standard deviation of RSSI at that location. The lowest signal strength for a broadcasting transmitter reflects the worst-case scenario considered in coverage analysis whereas the highest signal strength reflects the most optimistic scenario that provides valuable insights in interference analysis. With a variation map, a DST can handle high and low attenuation scenarios in a systematic, and deterministic manner.

An approach to quantify the variation of received signal strength is collecting empirical measurements and then either employing a fading model [75] to the data and estimating the model's parameters or conducting a statistical analysis, such as employing Allan variance [76]. However, these techniques require an extensive set of measurement samples for accurate estimation of model parameters and characterization of signal behavior.

A measurement map is necessary to obtain a variation map, unlike the expected signal strength map which can be obtained directly from a propagation map. The aggregation for signal variation can be achieved in various ways. If a small-scale averaging campaign is conducted at a set of proxels, the signal variation at these proxels can be predicted with the features associated with the signal variation. Once a model that is able to predict the measured variation is learned, it can be used to predict the variation throughout the map. This method is potentially the least costly method in terms of obtaining accurate variation predictions with the least amount of measurement samples.

However, in the usual scenario where there are no small-scale averaging measurements associated with a transmitter but only a single signal strength measurement is available at each measured proxel, two possible approaches can be utilized:

In the first approach, the measurement campaign is designed such that the denser, urban parts of the map are sampled more closely in space than the wider, constant land-use, semi-urban or rural locations that are less likely to have abrupt changes in fading behavior across space. With enough samples, the signal variation at a proxel can be captured by taking the variance of the measurements on a 2-dimensional kernel (mask) centered at that proxel. The kernel dimensions can be chosen to be smaller in dense urban environments, and larger in wider, rural environments such as agricultural lands, or deserts to capture accurate variation behavior.

In the second approach, if there are not enough measured proxels, the following set of steps can be taken to calculate discrete signal variation levels based on the measurements and extrapolate them throughout the map:

- The large-scale path loss is subtracted from signal strength measurements,
- The continuous features associated with variation are discretized,
- Signal variation is calculated for every combination of discrete features for which there exists an associated set of measurements,
- The resulting signal variation table is used to assign variations to proxels throughout the map based on the combination of features they have.

Several features associated with proxels can be used to quantify the expected amount of variation. These features may include the sight between a proxel and the transmitter (i.e., is the path line-of-sight (LOS) or non-line-of-sight (NLOS)), the amount of shadowing caused by a building obstructing the path, the distance from the transmitter, if the proxel is on a road aligned with the transmitter [77], and the number of obstacles obstructing the path from the transmitter causing multipath components to dominate the signal strength. An example signal variation table leveraging only two features affecting variation is illustrated in Table I where d is the distance to the stationary radio, and λ is a predetermined distance threshold.

	LOS	NLOS
d $< \lambda$	5.6	9.2
d $\geq \lambda$	7.8	10.1

TABLE I: An example signal variation table with discretized distance feature. Values show dB standard deviation.

Assuming received signal strength is independent for each transmitter, the overall signal strength variation map when multiple transmitters are operating can be obtained by linearly adding the variance of signal strength associated with each of m individual transmitters as shown in Equation (12). Even though fading can be correlated for different links having a common endpoint [78], the independence assumption provides a useful first-order analysis of potential variations.

$$\sigma^2(\sum_{i=1}^{m} RSS_i) = \sum_{i=1}^{m} \sigma^2(RSS_j) \tag{12}$$

C. Aggregation for Duty Cycle

An important factor in the planning of spectrum sharing is the periodicity of transmissions. Users of the spectrum may transmit during certain periods of the day (e.g., cellular radios) or have a listening interval during which no transmission occurs (e.g., pulsed transmitters). The estimated duty cycle map portrays the percentage of the time a transmission is expected at each proxel throughout the map.

The duty cycle information may be provided by the known set of transmitters as metadata with a notice to the DST each time this information changes for a given transmitter. Alternatively, if a spectrum monitoring infrastructure is set and used, the pattern obtained from current and historical measurements can be used to infer the periodicity and duty cycle associated with transmitters. Moreover, the changes in the duty cycle can be automatically noticed by the infrastructure in that case. The duty cycle associated with a transmitter inferred by an element of the infrastructure can be extrapolated to proxels within the coverage of that transmitter.

This work is licensed under a Creative Commons Attribution 4.0 License. For more information, see https://creativecommons.org/licenses/by/4.0/

This article has been accepted for publication in IEEE Journal of Radio Frequency Identification. This is the author's version which has not been fully edited and content may change prior to final publication. Citation information: DOI 10.1109/JRFID.2023.3327212

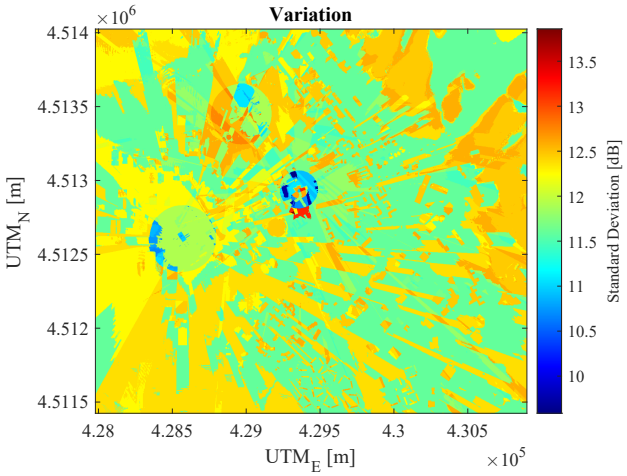

Fig. 7: Aggregated variation map obtained from three AMs based on two features, namely, distance to the transmitting radio and the shadowing angle of the mobile radio by the closest building in its vicinity. The individual variations are added for aggregation. The frequency of operation is 462.7 MHz in the UHF band.

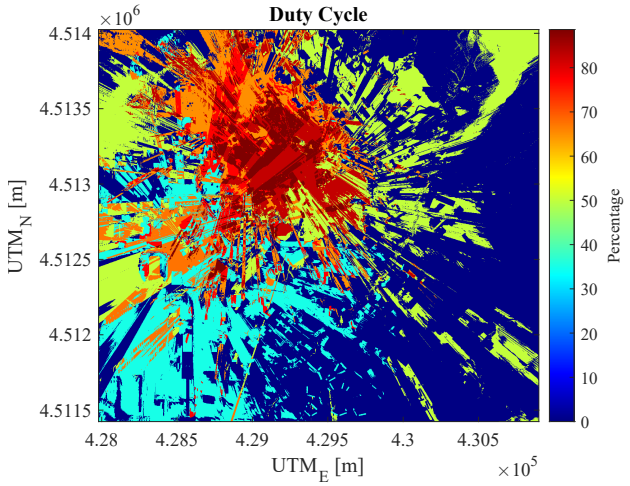

Fig. 8: Aggregated map of transmit duty cycle obtained from three known TXs for the Salt Lake City, UT area. The frequency of operation is 462.7 MHz in the UHF band.

A duty cycle information at a given location is only useful if the signal is detectable at that location. Therefore, a predetermined received signal strength value, η, set as the detection threshold determines the duty cycle of a given transmitter TX_j at a proxel p as shown in Equation (16):

$$D_p(TX_j) = \begin{cases} D_p & \text{if } RSS_{p,j} \geq \eta \\ 0 & \text{otherwise} \end{cases} \tag{13}$$

If a proxel p is within the coverage of multiple transmitters, the duty cycle at that proxel is lower-bounded by the maximum of the duty cycles (when the longest transmission overlaps with all other transmissions) and upper-bounded by the summation of the duty cycles (when transmissions do not overlap in time) as shown in Equation (14):

$$max(\{D_p(TX_j), \forall j \in S_{l,p}\}) \leq D_p \leq min(1, \sum_{j \in S_{l,p}} D_p(TX_j)) \tag{14}$$

where $S_{l,p}$ is an l-element set of transmitters detectable at proxel p. A single reference value for the duty cycle at proxel p can be obtained by Equation (15):

$$D_p = 1 - \prod_{j \in S_{l,p}} (1 - D_p(TX_j)) \tag{15}$$

D. Aggregation for Transmitter Type

Spectrum users make use of different types of technologies for their applications of interest. Some example technologies include radar (pulsed), cellular LTE and/or 5G-NR, WiFi, continuous wave (CW), and FM radio. The type of transmission may be an indicator of the priority of the users in a tiered access system. For instance, radar users are usually incumbent users and cellular LTE or 5G transmitters are priority access users in a CBRS-type of spectrum sharing scheme. It may also provide more context on the duty cycle as the duty cycle may convey different information depending on the type of transmission.

The information about the type of transmission can be provided by spectrum users as metadata. Otherwise, it can be deduced if radio-identification-based or coherent sensing is available and the transmission is an element of the known set of technologies or includes a subset of the known set of sequences.

The type of transmission map illustrates the classes of transmission throughout the map looked up from a table of all possible technologies. An example lookup table consisting of N different types of transmission having binary class numbers is illustrated in Table II.

Type of Transmission	Class
Radar (Pulsed)	$0 \ldots 00001 = 1$
FM Radio	$0 \ldots 00010 = 2$
CW	$0 \ldots 00100 = 4$
Cellular	$0 \ldots 01000 = 8$
WiFi	$0 \ldots 10000 = 16$
$\vdots$	$\vdots$
Bluetooth	$1 \ldots 00000 = 2^{N-1}$

TABLE II: An example lookup table for transmission classes.

If multiple transmissions affect a given proxel, the class at that proxel is calculated using the bitwise OR operation between individual class numbers. For instance, a class number of $0 \ldots 10011 = 19$ denotes that both pulsed, FM radio and WiFi transmissions affect the given proxel.

An alternative rule could be to use different prime numbers for different classes and to multiply different class numbers corresponding to different transmitters at the intersection of coverages. This approach would enable users to decode the number of transmitters of the same type affecting a given

This work is licensed under a Creative Commons Attribution 4.0 License. For more information, see https://creativecommons.org/licenses/by/4.0/

This article has been accepted for publication in IEEE Journal of Radio Frequency Identification. This is the author's version which has not been fully edited and content may change prior to final publication. Citation information: DOI 10.1109/JRFID.2023.3327212

proxel, unlike the binary approach that can only inform about the existence of a type of transmitter but not the number of transmitters of that type.

Similar to the duty cycle map, the transmitter type information is only useful when the transmission is detectable at the location of interest. Therefore,

$$T_p(TX_j) = \begin{cases} T_p & \text{if } RSS_{p,j} \geq \eta \\ 0 & \text{otherwise} \end{cases} \tag{16}$$

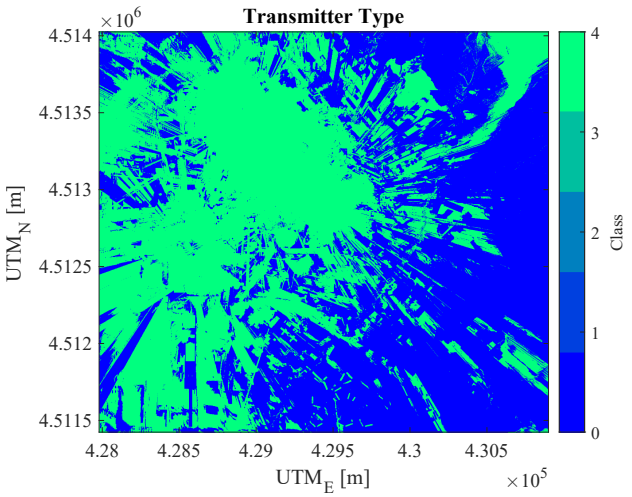

Fig. 9: Aggregated transmitter type map obtained from three KTXs for Salt Lake City, UT area. The frequency of operation is 462.7 MHz in the UHF band.

E. Aggregation for Confidence

The confidence map in the application layer illustrates the confidence in reported expected signal strength, variation, duty cycle, and transmitter type values. As the measured proxels offer ground-truth information, the confidence is significantly higher for proxels in closer proximity to these measurements. Therefore, distance, d_p, to the closest observed proxel plays an important role in confidence calculations. At proxels further away from the measurements, the confidence is mainly determined by the proxel-level accuracy of the propagation model's predictions, acc_p. One way of quantifying the confidence based on these factors is illustrated in Equation (17).

$$\begin{aligned} \gamma_p &= \beta(d_p)(1 - e^{-\alpha_1 acc_p}) + (1 - \beta(d_p))e^{-\alpha_2 d_p} \\ \beta(d_p) &= min(\frac{d_p}{d_{max}}, 1) \end{aligned} \tag{17}$$

where α_1, and α_2 determine the steepness of the exponential functions providing the freedom to prioritize closeness to measurements over propagation model's accuracy or vice versa. $\beta(d_p)$ is a parameter for weighting the propagation model's accuracy, and the distance to the closest observed proxel as a function of d_p.

The accuracy of the propagation model, acc_p reflects how close the predictions made by the propagation model are to the ground-truth measurements at a given proxel p. The deviation can be predicted at unobserved proxels with a regression model trained on observed deviations used also in the model tuning stage. Since the received signal strength is a random process, an accurate characterization of its statistics requires a certain amount of samples taken over time and space. In the ideal scenario where all proxels in the region are measured for a sufficient period of time, the confidence will be 100% for all proxels. Therefore, the number of measured proxels divided by the total number of proxels in the map, r, and the average number of samples among observed proxels, n_{avg}, dedicated to measurements in relation to some reference number of samples per observed proxel n_0 that is considered to be sufficient are also important factors affecting the confidence level. Therefore, an alternative formula for confidence can be calculated as shown in Equation (18):

$$\gamma_p^{'} = (1 - e^{-\alpha_3 \frac{n_{avg}}{n_0}})(1 - e^{-\alpha_4 r})\gamma_p \tag{18}$$

The confidence maps of individual transmitters can be aggregated with a minimum operator as shown in Equation (19):

$$\Gamma_p = min(\{\gamma_p(TX_j), \forall j \in S_{l,p}\}) \tag{19}$$

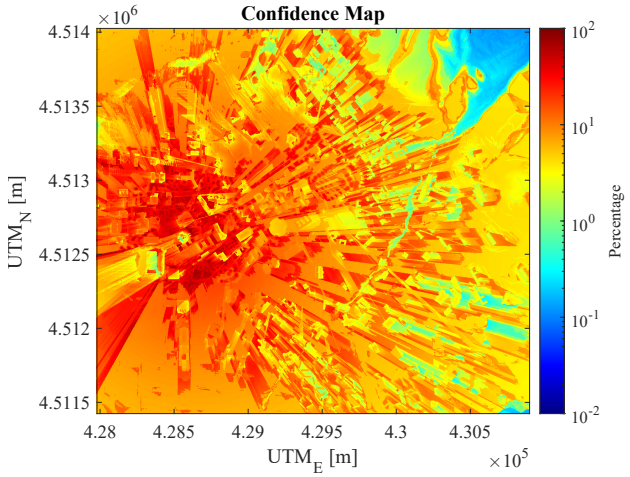

Fig. 10: Aggregated confidence map obtained from three KTXs for Salt Lake City, UT area. The frequency of operation is 462.7 MHz in the UHF band.

VI. Example Usage

In an example scenario where three known transmitters are operating in the POWDER platform on the University of Utah campus, a DST consisting of foundation, core, and application layers can be constructed based on the rules discussed.

Foundation Maps: The digital elevation map is combined with building heights in and around the campus at a region of size 2.6 km by 2.9 km to obtain the digital terrain profile as illustrated in Figure 11. The road orientation map is also generated for the region using the geographical information system (GIS) and Open-StreetMap (OSM) softwares.

Core Maps: The KTX map corresponding to each known transmitter is obtained using the TIREM propagation model

This work is licensed under a Creative Commons Attribution 4.0 License. For more information, see https://creativecommons.org/licenses/by/4.0/

This article has been accepted for publication in IEEE Journal of Radio Frequency Identification. This is the author's version which has not been fully edited and content may change prior to final publication. Citation information: DOI 10.1109/JRFID.2023.3327212

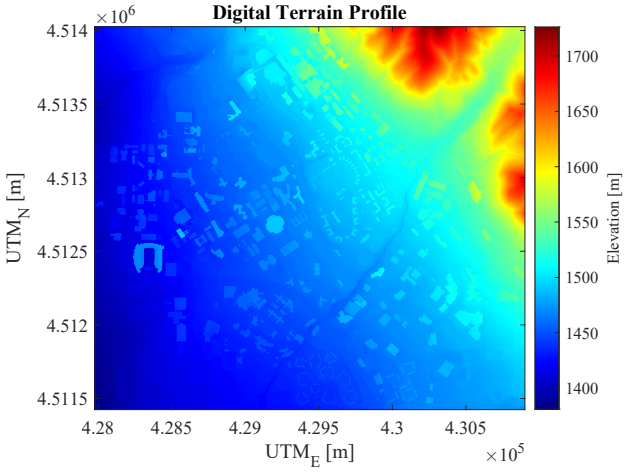

Fig. 11: Digital terrain profile showing a combination of the digital elevation map and the building layout in UTM zone 12. Map dimensions are approximately 2.6 km by 2.9 km with a 0.5 m resolution.

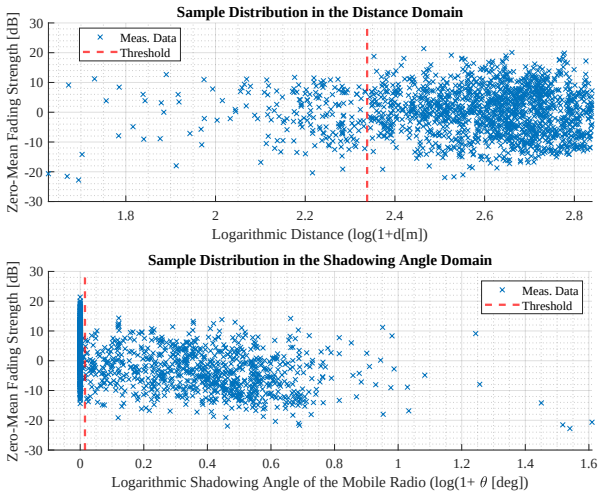

Fig. 12: Feature discretization thresholds for one transmitter determined based on the shifts in variation of sample distribution in their respective feature domains.

given the digital terrain profile and a few parameters such as transmitter and receiver heights, and environmental parameters. The AM maps were obtained from a measurement campaign [79] conducted on the POWDER platform [80], where a portable two-way radio (BaoFeng BF-F8HP) transmitted in the FRS band (462.7 MHz) while three rooftop radios were used to collect power measurements.

Application Maps: The KTX maps are individually tuned with the corresponding AM maps as the first step outlined in Equation (9). Consequently, AM maps were interpolated with an inpainting function that uses a method based on solving a partial differential equation (PDE) that is formulated over the field of the missing values [81]. The PDE is formulated such that it describes how a signal would propagate through the nearby region if it were excited at the boundaries. The boundary conditions are provided by the RSSI in measured proxels. A d_{max} value of 40 m is chosen and used in the interpolation and weighting steps. Finally, the tuned KTX, and the interpolated AM maps are weighted as a function of the distance to the closest measured proxel such that the final expected power map illustrated in Figure 6 is obtained.

The example variation maps are individually generated for each transmitter based on two proxel features, namely, distance to the transmitting radio, and the angle of shadowing of the mobile radio by the closest building in its vicinity which contains the sight (LOS vs. NLOS) information in it by definition. The large-scale path loss is subtracted from the measured RSSI values and the resulting zero-mean distribution of medium- and small-scale fading is used in the discretization of the features. This operation is performed based on the shifts observed in the variation of the zero-mean distribution of samples within their respective feature domains as depicted in Figure 12. The variations of samples having unique discrete feature combinations are calculated and a table of signal variation such as shown in Table I is generated. The process is repeated for all three terminals and the individual variation maps are aggregated based on Equation (12). The resulting variation map is illustrated in Figure 7.

The duty cycle and transmitter type maps are generated based on a detection threshold, η, determined to be -110 dBW. The three KTXs are assigned 35%, 50%, and 65% individual duty cycle values and aggregated according to Equation (15) whose result is shown in Figure 8. Since all three transmitters are continuous wave (CW) transmitters, their corresponding transmitter class is $0\ldots00100 = 4$ which is illustrated in Figure 9.

The individual confidence values are calculated using Equation (17) where the accuracy of the propagation model at proxel p, denoted as acc_p, is inversely related to the discrepancy between the predicted and actual loss values at that proxel. This value is quantified based on the magnitude of the extrapolated difference between the propagation model's prediction and the ground truth measurement. The parameters determining the steepness of the exponential functions are empirically chosen to be $\alpha_1 = 0.125$, and $\alpha_2 = 0.0625$. The individual maps are then aggregated with a minimum operator as stated in Equation (19).

VII. Conclusion

Digital spectrum twins provide a means to manage the radio spectrum more intelligently by first creating a digital twin of a geographic region in the foundation layer consisting of an elevation profile, building footprints and heights, ground use classification, and roadmaps. The collection of georeferenced maps in the foundation layer is then used in RF modeling and measurements across the region constituting the core layer. Efficient construction of core layer maps necessitates careful consideration regarding the selection of appropriate propagation models, measurement techniques, and sensing, detection, and localization methods. The generated propagation

This work is licensed under a Creative Commons Attribution 4.0 License. For more information, see https://creativecommons.org/licenses/by/4.0/

This article has been accepted for publication in IEEE Journal of Radio Frequency Identification. This is the author's version which has not been fully edited and content may change prior to final publication. Citation information: DOI 10.1109/JRFID.2023.3327212

and measurement maps in the core layer are finally aggregated into various maps in the application layer including expected signal power, variation, estimated duty cycle, confidence, and transmitter type maps. The information gathered in the application layer can be used to automate the decision-making process in spectrum sharing and management accommodating a greater number of radios thereby increasing the spectrum utilization efficiency [82]–[84].

More specifically, the expected power map can be used along with the variation map to analyze broadcast coverage in the environment as well as potential interference between different radio users and optimize the dynamic spectrum access problem. The duty cycle map along with the long-term traffic trends extracted from the DST can help systematically fill up the spectral vacancies both in time and physical space. The transmitter type map can inform decision-makers in terms of the priority of the users in a tiered spectrum access system while also providing context about the duty cycle information associated with the users. Confidence in these maps can be quantified by using the confidence map. The gathered application maps also pave the way for other services including the identification of rogue radio users, spectrum metering, and offering new location-based services for radios.

REFERENCES

[1] J. Breen, A. Buffmire, J. Duerig, K. Dutt, E. Eide, A. Ghosh, M. Hibler, D. Johnson, S. K. Kasera, E. Lewis, D. Maas, C. Martin, A. Orange, N. Patwari, D. Reading, R. Ricci, D. Schurig, L. B. Stoller, A. Todd, J. Van der Merwe, N. Viswanathan, K. Webb, and G. Wong, "POWDER: Platform for open wireless data-driven experimental research," *Computer Networks*, vol. 197, Oct. 2021, https://doi.org/10.1016/j.comnet.2021.108281. [Online]. Available: https://www.sciencedirect.com/science/article/pii/S1389128621003017

[2] G. D. Durgin, M. A. Varner, N. Patwari, S. K. Kasera, and J. Van der Merwe, "Digital spectrum twinning for next-generation spectrum management and metering," in *2022 IEEE 2nd International Conference on Digital Twins and Parallel Intelligence (DTPI)*, 2022, pp. 1–6.

[3] M. G. Weldegebriel, J. Wang, N. Zhang, and N. Patwari, "Pseudonymetry: Precise, private closed loop control for spectrum reuse with passive receivers," in *2022 IEEE International Conference on RFID (RFID)*, 2022, pp. 91–96.

[4] R. H. Tehrani, S. Vahid, D. Triantafyllopoulou, H. Lee, and K. Moessner, "Licensed spectrum sharing schemes for mobile operators: A survey and outlook," *IEEE Communications Surveys Tutorials*, vol. 18, no. 4, pp. 2591–2623, 2016.

[5] Y. Qu, C. Dong, S. Tang, C. Chen, H. Dai, H. Wang, and C. Tian, "Opportunistic network coding for secondary users in cognitive radio networks," *Ad Hoc Networks*, vol. 56, pp. 186–201, 2017. [Online]. Available: https://www.sciencedirect.com/science/article/pii/S1570870516303377

[6] Y. Xu, J. Wang, Q. Wu, A. Anpalagan, and Y.-D. Yao, "Opportunistic spectrum access in unknown dynamic environment: A game-theoretic stochastic learning solution," *IEEE Transactions on Wireless Communications*, vol. 11, no. 4, pp. 1380–1391, 2012.

[7] D. Niyato and E. Hossain, "Cognitive radio for next-generation wireless networks: an approach to opportunistic channel selection in ieee 802.11-based wireless mesh," *IEEE Wireless Communications*, vol. 16, no. 1, pp. 46–54, 2009.

[8] H.-P. Shiang and M. van der Schaar, "Queuing-based dynamic channel selection for heterogeneous multimedia applications over cognitive radio networks," *IEEE Transactions on Multimedia*, vol. 10, no. 5, pp. 896–909, 2008.

[9] T. Baykas, M. Kasslin, M. Cummings, H. Kang, J. Kwak, R. Paine, A. Reznik, R. Saeed, and S. J. SHELLHAMMER, "Developing a standard for tv white space coexistence: technical challenges and solution approaches," *IEEE Wireless Communications*, vol. 19, no. 1, pp. 10–22, 2012.

[10] "Response to the industry canada consultation on a policy and technical framework for the use of non-broadcasting applications in the television broadcasting bands below 698 MHz," *IEEE 802.18 Radio Regulatory Technical Advisory Group*, Oct 2011. [Online]. Available: https://mentor.ieee.org/802.18/dcn/11/18-11-0075-04-0000-ieee-802-response-to-canadian-tvws-consultation.doc

[11] M. M. Sohul, M. Yao, T. Yang, and J. H. Reed, "Spectrum access system for the citizen broadband radio service," *IEEE Communications Magazine*, vol. 53, no. 7, pp. 18–25, 2015.

[12] "Fcc takes next step to enable faster, better wi-fi," https://www.fcc.gov/document/fcc-takes-next-step-enable-faster-better-wi-fi, accessed: 2023-06-24.

[13] Y. Okumura, E. Ohmori, T. Kawano, and K. Fukuda, "Field strength and its variability in vhf and uhf land-mobile radio service," *Rev. Electr. Commun. Lab.*, vol. 16, pp. 825–873, 1968.

[14] M. Hata, "Empirical formula for propagation loss in land mobile radio services," *IEEE Transactions on Vehicular Technology*, vol. 29, no. 3, pp. 317–325, 1980.

[15] G. A. Hufford, A. G. Longley, and W. A. Kissick, "A guide to the use of the ITS irregular terrain model in the area prediction mode," p. 13351, Apr. 1982.

[16] D. Eppink and W. Kuebler, *TIREM/SEM Handbook*. IIT Research Institute, Tech. Rep., Sept 1986.

[17] Z. Yun and M. F. Iskander, "Ray tracing for radio propagation modeling: Principles and applications," *IEEE Access*, vol. 3, pp. 1089–1100, 2015.

[18] S. Tadik, M. A. Varner, F. Mitchell, and G. D. Durgin, "Augmented rf propagation modeling," *IEEE Journal of Radio Frequency Identification*, pp. 1–1, 2023.

[19] M. A. Varner, F. Mitchell, J. Wang, K. Webb, and G. D. Durgin, "Enhanced rf modeling accuracy using simple minimum mean-squared error correction factors," in *2022 IEEE 2nd International Conference on Digital Twins and Parallel Intelligence (DTPI)*, 2022, pp. 1–5.

[20] R. I. C. Chiang, G. B. Rowe, and K. W. Sowerby, "A quantitative analysis of spectral occupancy measurements for cognitive radio," in *2007 IEEE 65th Vehicular Technology Conference - VTC2007-Spring*, 2007, pp. 3016–3020.

[21] S. Yin, D. Chen, Q. Zhang, M. Liu, and S. Li, "Mining spectrum usage data: A large-scale spectrum measurement study," *IEEE Transactions on Mobile Computing*, vol. 11, no. 6, pp. 1033–1046, 2012.

[22] M. H. Islam, C. L. Koh, S. W. Oh, X. Qing, Y. Y. Lai, C. Wang, Y.-C. Liang, B. E. Toh, F. Chin, G. L. Tan, and W. Toh, "Spectrum survey in singapore: Occupancy measurements and analyses," in *2008 3rd International Conference on Cognitive Radio Oriented Wireless Networks and Communications (CrownCom 2008)*, 2008, pp. 1–7.

[23] D. Chen, J. Yang, J. Wu, H. Tang, and M. Huang, "Spectrum occupancy analysis based on radio monitoring network," in *2012 1st IEEE International Conference on Communications in China (ICCC)*, 2012, pp. 739–744.

[24] May 2021. [Online]. Available: https://www.sharedspectrum.com/technologies/dynamic-spectrum-access/

[25] A. Chakraborty, A. Bhattacharya, S. Kamal, S. R. Das, H. Gupta, and P. M. Djuric, "Spectrum patrolling with crowdsourced spectrum sensors," in *IEEE INFOCOM 2018 - IEEE Conference on Computer Communications*, 2018, pp. 1682–1690.

[26] Y. Lin, Y. Ye, and Y. Yang, "Crowdsourcing-based spectrum monitoring at a large geographical scale," in *2019 IEEE International Symposium on Dynamic Spectrum Access Networks (DySPAN)*, 2019, pp. 1–10.

[27] Y. Chen and A. Terzis, "On the mechanisms and effects of calibrating RSSI measurements for 802.15.4 radios," in *7th European Conference on Wireless Sensor Networks (EWSN 2010)*, 2010, pp. 256–271.

[28] A. Nika, Z. Zhang, X. Zhou, B. Y. Zhao, and H. Zheng, "Towards commoditized real-time spectrum monitoring," in *Proceedings of the 1st ACM Workshop on Hot Topics in Wireless*, ser. HotWireless '14. New York, NY, USA: Association for Computing Machinery, 2014, p. 25–30. [Online]. Available: https://doi.org/10.1145/2643614.2643615

[29] A. Chakraborty, M. S. Rahman, H. Gupta, and S. R. Das, "Specsense: Crowdsensing for efficient querying of spectrum occupancy," in *IEEE INFOCOM 2017 - IEEE Conference on Computer Communications*, 2017, pp. 1–9.

[30] C. H. Liu, J. Fan, P. Hui, J. Wu, and K. K. Leung, "Toward qoi and energy efficiency in participatory crowdsourcing," *IEEE Transactions on Vehicular Technology*, vol. 64, no. 10, pp. 4684–4700, 2015.

This work is licensed under a Creative Commons Attribution 4.0 License. For more information, see https://creativecommons.org/licenses/by/4.0/

This article has been accepted for publication in IEEE Journal of Radio Frequency Identification. This is the author's version which has not been fully edited and content may change prior to final publication. Citation information: DOI 10.1109/JRFID.2023.3327212

[31] C. H. Liu, B. Zhang, X. Su, J. Ma, W. Wang, and K. K. Leung, "Energy-aware participant selection for smartphone-enabled mobile crowd sensing," *IEEE Systems Journal*, vol. 11, no. 3, pp. 1435–1446, 2017.

[32] W. Wang, H. Gao, C. H. Liu, and K. K. Leung, "Credible and energy-aware participant selection with limited task budget for mobile crowd sensing," *Ad Hoc Networks*, vol. 43, pp. 56–70, 2016, smart Wireless Access Networks and Systems for Smart Cities. [Online]. Available: https://www.sciencedirect.com/science/article/pii/S1570870516300300

[33] Y. Zhang and M. van der Schaar, "Robust reputation protocol design for online communities: A stochastic stability analysis," *IEEE Journal of Selected Topics in Signal Processing*, vol. 7, no. 5, pp. 907–920, 2013.

[34] G. D. Durgin, M. A. Varner, M. A. Weitnauer, J. Cressler, M. M. Tentzeris, A. Zajic, S. Zeinolabedinzadeh, R. Zekavat, K. Pahlavan, U. Guler, and K. Van der Merwe, "Digital spectrum twinning and the role of RFID and backscatter communications in spectral sensing," in *2021 IEEE International Conference on RFID Technology and Applications (RFID-TA)*, 2021, pp. 89–92.

[35] M. Usman and K. Insoo, "Sensor network-based spectrum sensing for cognitive radio network," in *2016 International Conference on Intelligent Systems Engineering (ICISE)*, 2016, pp. 19–25.

[36] J. Naganawa, H. Kim, S. Saruwatari, H. Onaga, and H. Morikawa, "Distributed spectrum sensing utilizing heterogeneous wireless devices and measurement equipment," in *2011 IEEE International Symposium on Dynamic Spectrum Access Networks (DySPAN)*, 2011, pp. 173–184.

[37] A. P. Iyer, K. Chintalapudi, V. Navda, R. Ramjee, V. N. Padmanabhan, and C. R. Murthy, "SpecNet: Spectrum sensing sans Frontières," in *8th USENIX Symposium on Networked Systems Design and Implementation (NSDI 11)*. Boston, MA: USENIX Association, Mar. 2011. [Online]. Available: https://www.usenix.org/conference/nsdi11/specnet-spectrum-sensing-sans-frontières

[38] A. Ghasemi and E. S. Sousa, "Spectrum sensing in cognitive radio networks: requirements, challenges and design trade-offs," *IEEE Communications Magazine*, vol. 46, no. 4, pp. 32–39, 2008.

[39] P. Sharma and V. Abrol, "Individual vs cooperative spectrum sensing for cognitive radio networks," in *2013 Tenth International Conference on Wireless and Optical Communications Networks (WOCN)*, 2013, pp. 1–5.

[40] A. Giorgetti and K. Sithamparanathan, *Cognitive Radios Techniques: Spectrum Sensing, Interference Mitigation and Localization*, 2012.

[41] S. Hussain and X. Fernando, "Spectrum sensing in cognitive radio networks: Up-to-date techniques and future challenges," in *2009 IEEE Toronto International Conference Science and Technology for Humanity (TIC-STH)*, 2009, pp. 736–741.

[42] A. Molisch, *Wireless Communications*, 2nd ed. Wiley-IEEE Press, 2011.

[43] C. Dietrich, K. Dietze, J. Nealy, and W. Stutzman, "Spatial, polarization, and pattern diversity for wireless handheld terminals," *IEEE Transactions on Antennas and Propagation*, vol. 49, no. 9, pp. 1271–1281, 2001.

[44] K. M. Graves, M. A. Varner, and G. D. Durgin, "Low-power rfid enabled bistatic reflect antenna array for small-scale fading mitigation," in *2023 IEEE International Conference on RFID*, 2023, pp. 60–65.

[45] A. Ghasemi and E. Sousa, "Collaborative spectrum sensing for opportunistic access in fading environments," in *First IEEE International Symposium on New Frontiers in Dynamic Spectrum Access Networks, 2005. DySPAN 2005.*, 2005, pp. 131–136.

[46] T. Yucek and H. Arslan, "A survey of spectrum sensing algorithms for cognitive radio applications," *IEEE Communications Surveys Tutorials*, vol. 11, no. 1, pp. 116–130, 2009.

[47] H. Urkowitz, "Energy detection of unknown deterministic signals," *Proceedings of the IEEE*, vol. 55, no. 4, pp. 523–531, 1967.

[48] D. Cabric, S. Mishra, and R. Brodersen, "Implementation issues in spectrum sensing for cognitive radios," in *Conference Record of the Thirty-Eighth Asilomar Conference on Signals, Systems and Computers, 2004.*, vol. 1, 2004, pp. 772–776 Vol.1.

[49] E. Axell, G. Leus, E. G. Larsson, and H. V. Poor, "Spectrum sensing for cognitive radio : State-of-the-art and recent advances," *IEEE Signal Processing Magazine*, vol. 29, no. 3, pp. 101–116, 2012.

[50] A. Ali and W. Hamouda, "Advances on spectrum sensing for cognitive radio networks: Theory and applications," *IEEE Communications Surveys Tutorials*, vol. 19, no. 2, pp. 1277–1304, 2017.

[51] H. Urkowitz, "Energy detection of unknown deterministic signals," *Proceedings of the IEEE*, vol. 55, no. 4, pp. 523–531, 1967.

[52] I. Sobron, P. S. R. Diniz, W. A. Martins, and M. Velez, "Energy detection technique for adaptive spectrum sensing," *IEEE Transactions on Communications*, vol. 63, no. 3, pp. 617–627, 2015.

[53] F. F. Digham, M.-S. Alouini, and M. K. Simon, "On the energy detection of unknown signals over fading channels," *IEEE Transactions on Communications*, vol. 55, no. 1, pp. 21–24, 2007.

[54] H. Tang, "Some physical layer issues of wide-band cognitive radio systems," in *First IEEE International Symposium on New Frontiers in Dynamic Spectrum Access Networks, 2005. DySPAN 2005.*, 2005, pp. 151–159.

[55] D. Cabric, A. Tkachenko, and R. W. Brodersen, "Spectrum sensing measurements of pilot, energy, and collaborative detection," in *MILCOM 2006 - 2006 IEEE Military Communications conference*, 2006, pp. 1–7.

[56] Y. Zhu, J. Liu, Z. Feng, and P. Zhang, "Sensing performance of efficient cyclostationary detector with multiple antennas in multipath fading and lognormal shadowing environments," *Journal of Communications and Networks*, vol. 16, no. 2, pp. 162–171, 2014.

[57] G. Huang and J. K. Tugnait, "On cyclostationarity based spectrum sensing under uncertain gaussian noise," *IEEE Transactions on Signal Processing*, vol. 61, no. 8, pp. 2042–2054, 2013.

[58] W. Gardner, "Exploitation of spectral redundancy in cyclostationary signals," *IEEE Signal Processing Magazine*, vol. 8, no. 2, pp. 14–36, 1991.

[59] A. Fehske, J. Gaeddert, and J. Reed, "A new approach to signal classification using spectral correlation and neural networks," in *First IEEE International Symposium on New Frontiers in Dynamic Spectrum Access Networks, 2005. DySPAN 2005.*, 2005, pp. 144–150.

[60] S. Haykin, D. J. Thomson, and J. H. Reed, "Spectrum sensing for cognitive radio," *Proceedings of the IEEE*, vol. 97, no. 5, pp. 849–877, 2009.

[61] F. Nawaz, A. Akanser, S. A. Hassan, and M. A. Weitnauer, "Wireless one-shot polling of a cluster of sensors using transmit diversity," in *2018 IEEE 87th Vehicular Technology Conference (VTC Spring)*, 2018, pp. 1–5.

[62] E. Ghunney, S. A. Hassan, and M. A. Weitnauer, "Impact of wrong beam selection on beam pair scanning method for user discovery in mmwave systems," in *2020 IEEE 91st Vehicular Technology Conference (VTC2020-Spring)*, 2020, pp. 1–5.

[63] A. C. Djedouboum, A. A. Abba Ari, A. M. Gueroui, A. Mohamadou, and Z. Aliouat, "Big data collection in large-scale wireless sensor networks," *Sensors*, vol. 18, no. 12, 2018. [Online]. Available: https://www.mdpi.com/1424-8220/18/12/4474

[64] J. P. Snyder, "Map projections used by the u.s. geological survey," Washington, D.C., Tech. Rep., 1982, report. [Online]. Available: http://pubs.er.usgs.gov/publication/b1532

[65] J. Talvitie and E. S. Lohan, "Modeling received signal strength measurements for cellular network based positioning," in *2013 International Conference on Localization and GNSS (ICL-GNSS)*, 2013, pp. 1–6.

[66] D. Madariaga, J. Madariaga, J. Bustos-Jiménez, and B. Bustos, "Improving signal-strength aggregation for mobile crowdsourcing scenarios," *Sensors*, vol. 21, no. 4, 2021. [Online]. Available: https://www.mdpi.com/1424-8220/21/4/1084

[67] M. Molinari, M.-R. Fida, M. K. Marina, and A. Pescape, "Spatial interpolation based cellular coverage prediction with crowdsourced measurements," ser. C2B(1)D '15. New York, NY, USA: Association for Computing Machinery, 2015, p. 33–38. [Online]. Available: https://doi.org/10.1145/2787394.2787395

[68] M.-R. Fida, A. Lutu, M. K. Marina, and Alay, "Zipweave: Towards efficient and reliable measurement based mobile coverage maps," in *IEEE INFOCOM 2017 - IEEE Conference on Computer Communications*, 2017, pp. 1–9.

[69] I. Santos, J. J. Murillo-Fuentes, and P. M. Djurić, "Recursive estimation of dynamic rss fields based on crowdsourcing and gaussian processes," *IEEE Transactions on Signal Processing*, vol. 67, no. 5, pp. 1152–1162, 2019.

[70] C. Zhan, H. Gupta, A. Bhattacharya, and M. Ghaderibaneh, "Efficient localization of multiple intruders in shared spectrum system," in *2020 19th ACM/IEEE International Conference on Information Processing in Sensor Networks (IPSN)*, 2020, pp. 205–216.

[71] A. Zubow, S. Bayhan, P. Gawłowicz, and F. Dressler, "Deeptxfinder: Multiple transmitter localization by deep learning in crowdsourced spectrum sensing," in *2020 29th International Conference on Computer Communications and Networks (ICCCN)*, 2020, pp. 1–8.

This work is licensed under a Creative Commons Attribution 4.0 License. For more information, see https://creativecommons.org/licenses/by/4.0/

This article has been accepted for publication in IEEE Journal of Radio Frequency Identification. This is the author's version which has not been fully edited and content may change prior to final publication. Citation information: DOI 10.1109/JRFID.2023.3327212

[72] R. K. Martin and R. Thomas, "Algorithms and bounds for estimating location, directionality, and environmental parameters of primary spectrum users," *IEEE Transactions on Wireless Communications*, vol. 8, no. 11, pp. 5692–5701, 2009.

[73] M. Khaledi, M. Khaledi, S. Sarkar, S. Kasera, N. Patwari, K. Derr, and S. Ramirez, "Simultaneous power-based localization of transmitters for crowdsourced spectrum monitoring," in *Proceedings of the 23rd Annual International Conference on Mobile Computing and Networking*, ser. MobiCom '17. New York, NY, USA: Association for Computing Machinery, 2017, p. 235–247. [Online]. Available: https://doi.org/10.1145/3117811.3117845

[74] C. Zhan, M. Ghaderibaneh, P. Sahu, and H. Gupta, "Deepmtl pro: Deep learning based multiple transmitter localization and power estimation," *Pervasive and Mobile Computing*, vol. 82, p. 101582, 2022. [Online]. Available: https://www.sciencedirect.com/science/article/pii/S1574119222000311

[75] G. Durgin, *Space-Time Wireless Channels*, 1st ed. USA: Prentice Hall Press, 2002.

[76] C. Luo, P. Casaseca-de-la Higuera, S. McClean, G. Parr, and P. Ren, "Characterization of received signal strength perturbations using allan variance," *IEEE Transactions on Aerospace and Electronic Systems*, vol. 54, no. 2, pp. 873–889, 2018.

[77] G. D. Durgin, "Electro-magnetic propagation modeling," U.S. Patent 7 433 652 B2, Oct. 7, 2008.

[78] P. Agrawal and N. Patwari, "Correlated link shadow fading in multi-hop wireless networks," *IEEE Transactions on Wireless Communications*, vol. 8, no. 8, pp. 4024–4036, 2009.

[79] F. Mitchell, A. Baset, S. K. Kasera, and A. Bhaskara, "A Dataset of Outdoor RSS Measurements for Localization," Oct. 2022. [Online]. Available: https://doi.org/10.5281/zenodo.7259895

[80] J. Breen, A. Buffmire, K. D. J. Duerig, M. H. E. Eide, S. K. K. D. Johnson, D. M. E. Lewis, A. Orange, N. Patwari, D. Reading, R. Ricci, D. Schurig, L. B. Stoller, J. V. der Merwe, K. Webb, and G. Wong., "Powder: Platform for open wireless data-driven experimental research," in *14th International Workshop on Wireless Network Testbeds, Experimental Evaluation and Characterization (WiNTECH)*, September 2020.

[81] J. D'Errico, "inpaint_nans," https://www.mathworks.com/matlabcentral/fileexchange/4551-inpaint_nans, 2023, mATLAB Central File Exchange.

[82] G. D. Durgin, Ed., *BESTNEST Workshop on Intelligent Radio*, https://bestnest.wpi.edu/index.php/synapsis-2/, 2020.

[83] S. Zekavat, Ed., *Intelligent Radio: A Gateway to a Comprehensive Spectrum Twinning*, IEEE RFID 2022 Workshop on Digital Spectrum Twinning, 2022.

[84] A. Drobot, Ed., *The Digital Spectrum Twin: The Path to Achieving Realtime Efficient Spectrum Sharing.*, IEEE RFID 2022 Workshop on Digital Spectrum Twinning, 2022.

This work is licensed under a Creative Commons Attribution 4.0 License. For more information, see https://creativecommons.org/licenses/by/4.0/